

<https://doi.org/10.22201/igeof.00167169p.2022.61.4.2203>

Modelling of Residual Gravity Data due to a Near Surface Dyke Structure Using Damped SVD and Marquardt Inverse Methods

Ata Eshaghzadeh^{1*} , Alireza Hajian²

Received: December 8, 2021; accepted: August 16, 2022; published on-line: October 1, 2022.

RESUMEN

En este artículo, se describen dos métodos de modelado inverso basados en la descomposición de valor singular amortiguado (DSVD) como inversor lineal y el algoritmo de optimización de Marquardt como inversor no lineal. El SVD amortiguado resuelve los problemas mal planteados y especifica directamente la contribución de la densidad de la superficie inferior. La inversión de Marquardt estima los parámetros del modelo. La eficiencia de ambos métodos se investiga utilizando los datos de gravedad sintéticos, con y sin ruido aleatorio, según se obtengan los resultados aceptables. Los enfoques introducidos se emplean para la interpretación de un conjunto de datos de gravedad real de Irán. La masa causante de la gravedad en el área de estudio son casi el depósito magmático con un alto porcentaje de dióxido de manganeso donde han penetrado dentro de las fracturas y aproximadamente se han formado las estructuras tabulares. Las estructuras invertidas de ambos métodos son casi correspondientes. El ancho, la extensión y la profundidad evaluados hasta la parte superior e inferior de la estructura enterrada mediante la técnica SVD amortiguada son 15 m, 22 m, 7.5 m y 25 m, respectivamente, y según el algoritmo de Marquardt son 15.8 m, 20.3 m, 9.4 m y 21.9 m, respectivamente. La fuente simulada tiene una tendencia NW-SE con una caída de 38,04 grados.

PALABRAS CLAVE: descomposición amortiguada en valor singular, gravedad y Marquardt

Editorial responsibility: Juan García-Abdeslem

**Corresponding author at eshagh@ut.ac.ir*

¹Department of Geology, Faculty of Sciences, University of Isfahan, Isfahan, Iran

²Department of physics, Najafabad Branch, Islamic Azad University, Najafabad, Iran

ABSTRACT

In this paper, two inverse modeling methods based on the damped singular value decomposition (DSVD) as a linear inverter and Marquardt optimization algorithm as a nonlinear inverter are described. The damped SVD solve the ill-posed problems and specify the subsurface density contribution directly. The Marquardt inversion estimate the model parameters. The efficiency of the both methods is investigated using the synthetic gravity data, with and without random noise, as the acceptable results attained. The introduced approaches are employed for the interpretation of a real gravity data set from Iran. The gravity causative mass in the study area are almost the magmatic deposit with a high percent of the Manganese dioxide where there have penetrated inside of the fractures and have approximately formed the tabular structures. The inverted structures from the both methods are almost corresponding. The evaluated width, extension and depth to the top and bottom for the buried structure via the damped SVD technique are 15 m, 22 m, 7.5 m and 25 m, respectively and by the Marquardt's algorithm are 15.8 m, 20.3 m, 9.4 m and 21.9 m, respectively. The simulated source has a trend NW-SE with a dip of 38.04 degree.

KEY WORDS: damped singular value decomposition (DSVD), gravity and Marquardt

INTRODUCTION

Gravity investigation plays an important role in geological studies and has been used widely over the years for modeling buried geological structures and deposit, especially in mineral reconnaissance projects. The non-uniqueness in the linear inverse problem of gravity, i.e., the existence of a large variety of distribution of subsurface density distribution models that generate a similar gravity effect on measurement plane, makes one to hesitate on the reliability of solution (Skeels, 1947; Parker, 1972). In order to obtain a correct unique solution and to decrease the ambiguities, various researchers have been proposed different algorithms to increase the amount of extracted information from inversion for simulating the geometry of a density distribution related to a known gravity anomaly, such that the proposed model be geologically realistic.

Tsuboi (1983) introduced a simple but effective approach based on the equivalent stratum technique to estimate 3D topography of a density interface. Oldenburg (1974) proved that the Parker's expression could be applied in order to specify the geometry of the density interface from its gravity anomaly. The geological maps and petrophysical data from rock samples were used to constraint the model parameters to realistic values (Farquharson *et al.*, 2008; Williams, 2008; Heincke *et al.*, 2010; Lelièvre *et al.*, 2012; Tschirhart *et al.*, 2013, 2017). Kamm *et al.* (2015) used the petrophysical information conduct a joint inversion of gravity and magnetic data. Ialongo *et al.* (2014) show that there are invariant models in the inversion of gravity and magnetic fields and their derivatives.

Using a joint inversion of multiple data sets can also diminish the nonuniqueness of the inverse problem. examples of joint inversion of gravity and magnetic data are given by, e.g., Zeyen and Pous (1993), Gallardo and Meju (2003), and Pilkington (2006) using deterministic inversion techniques and by Bosch and McGaughey (2001), Bosch *et al.* (2006) and Shamsipour *et al.* (2012) using stochastic methods. Shamsipour *et al.* (2010, 2011, 2012) proposed geostatistical techniques of cokriging and conditional simulation for the separate three-dimensional inversion of gravity and magnetic data respectively, including geological constraints.

One way to eliminate the inherent ambiguity is to propose a geologically sound geometry as the source of the anomalous body with a known density as the start point of the inversion of gravity

anomalies (Chakravarthi and Sundararajan, 2004). Although simple models may not be geologically realistic, they usually are sufficient to analyze sources of many isolated anomalies (Abdelrahman and El-Araby, 1993). The interpretation of a given anomaly aims essentially to estimate the parameters such as shape, depth, radius, thickness and so on. Thus, in this case it is dealt with nonlinear inverse modeling. The many of the proposed nonlinear techniques are based on an initial guess of the geological structure parameters, 1) in the case of least-squares minimization approaches (Gupta, 1983; Lines and Treitel, 1984; Abdelrahman, 1990; Abdelrahman *et al.*, 1991; Asfahani and Tlas, 2007, 2008) 2) different neural networks (Eslam *et al.*, 2001; Osman *et al.*, 2006 and 2007; Al-garni *et al.*, 2013; Eshaghzadeh and Kalantari, 2015; Eshaghzadeh and Hajian, 2018); 3) Continual least squares methods (Abdelrahman and Sharafeldin 1996; Abdelrahman *et al.* 2001, 2001a, 2001b; Essa 2012, 2013); 4) effective quantitative interpretations using the least-squares method based on the analytical expression of simple moving average residual gravity anomalies (Gupta, 1983; Abdelrahman *et al.* 2003, 2007, 2015). Appraisal of the depth and shape of a buried structure from the observed gravity and gravity data is widely used in exploration operations, in methods based on the Fourier transform (Odegard and Berg, 1965; Sharma and Geldart, 1968); Mellin transform (Mohan *et al.* 1986); Walsh transforms techniques (Shaw and Agarwal, 1990); ratio techniques (Hammer, 1977; Abdelrahman *et al.*, 1989; Cooper, 2012; Eshaghzadeh, 2017).

Dyke is a sheet-like geological structure generated from intrusive igneous rock while cut through the strata. Dyke structure has different slopes, thicknesses and lateral dimension extent. Structures that have a higher density contrast than that of their encasing formation as are easily detectable in the residual gravity field maps. Because of existence the important minerals in the igneous rock, such as chromite, magnetite and so on, these tabular structures are among the very considerable exploratory targets in geophysical investigations, especially when based on potential fields methods.

By searching many papers related to our subject it can be found that their focus is on determining the parameters of dyke-like gravity sources (Bastani and Pedersen 2001; Abdelrahman and Essa 2007; Abdelrahman *et al.* 2003, Asfahani and Tlas 2007; Tlas and Asfahani 2011a, b; Cooper 2012, 2014, 2015; Abdelrahman *et al.* 2015) while it can be stated that dyke non-linear inverse modeling from gravity data less has been investigated. Ateya and Takemoto (2002) proposed a gravity inversion modeling across a 2-D dike-like structure. A fast simulated annealing global optimization technique has been proposed by Biswas (2016) to the interpretation of gravity and gravity anomaly over thin sheet-type structure. Biswas *et al.* (2017) also applied a nonlinear optimization method for the determination of dyke-type source parameters based on the calculation of first order horizontal and vertical derivatives of the gravity and gravity anomalies. Peace *et al.* (2018) employed the full tensor gravimetry (FTG) data for 3-D subsurface models of the Budgetell Harbour Stock and associated dykes, Newfoundland, Canada. Abdelfattah *et al.* (2021) performed an integrated analysis based on gravity and seismological data with focusing on the HL seismogenic and volcanic zone in the western shield of Saudi Arabia, which has a complex structure comprises dykes, recent volcanic eruptions, and fault segments of various orientations.

For first one, in this study, we employ the linear inverse modeling technique based on the damped singular value decomposition (DSVD) and using a depth weighting parameter as resolution enhancer and a two-norm (also known as the L2 norm or least squares) as stopping criteria in inversion algorithms. SVD constitutes a famous and numerically stable method for analyzing the underdetermined problems, i.e. ill-condition matrices, and is a standard technique for small inverse problems.

We also develop the Marquardt’s algorithm (1963) for inverting the 2-D observed gravity anomaly due to finite dyke-shape model in order to evaluate the depth to top, height (the depth to bottom is estimated), width and slope of buried structure. We exemplify the capability of the both methods by a theoretical model with and without a random noise. Finally, these inversion techniques are employed for the interpretation of the real gravity data from Iran.

COMPUTING THE KERNEL MATRIX

For inverting the gravity data for calculating a 2D density distribution, it is necessary that the sub-surface be divided in order to calculate the gravity effect of the obtained density distribution at the surface. For a 2D model, as shown in Figure 1, the gravity effect of all the rectangular blocks at the observation point i , is given by:

$$g_i = \sum_{j=1}^M P_{ij} d_j, \quad i = 1, \dots, N \tag{1}$$

where M and N denote the number of blocks and the number of observations, respectively, d_j is the density of the j^{th} block and P_{ij} is matrix of geometric element or kernel matrix which presenting the influence of the j^{th} block on the i^{th} gravity value. In order to calculate the kernel matrix P_{ij} , the gravity response of the 2D prism is based on the equation developed by Last and Kubik (1983):

$$P_{ij} = 2G \begin{bmatrix} \left(x_1 - x_j + \frac{d}{2} \right) \log \left(\frac{r_2 r_3}{r_1 r_4} \right) + d \log \left(\frac{r_4}{r_3} \right) - \\ \left(z_j + \frac{h}{2} \right) (\theta_4 - \theta_2) + \left(z_j - \frac{h}{2} \right) (\theta_3 - \theta_1) \end{bmatrix} \tag{2}$$

where

$$r_1^2 = \left(z_j - \frac{h}{2} \right)^2 + \left(x_1 - x_j + \frac{d}{2} \right)^2$$

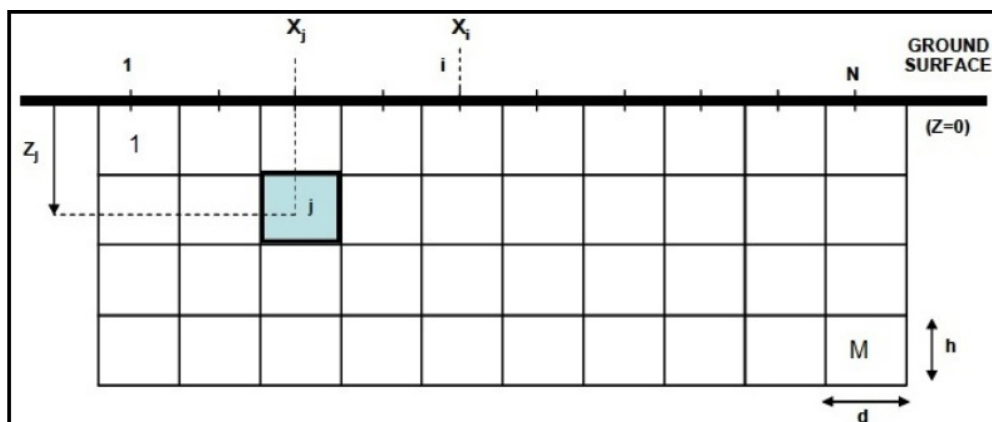


Figure 1. A 2-D schematic view of the inversion domain divided into several blocks as the gravity stations are located at the center of the blocks at the ground surface.

$$r_2^2 = \left(z_j - \frac{h}{2}\right)^2 + \left(x_1 - x_j + \frac{d}{2}\right)^2$$

$$r_3^2 = \left(z_j - \frac{h}{2}\right)^2 + \left(x_1 - x_j + \frac{d}{2}\right)^2$$

$$r_4^2 = \left(z_j - \frac{h}{2}\right)^2 + \left(x_1 - x_j + \frac{d}{2}\right)^2$$

and

$$\theta_1 = \tan^{-1} \left(x_i - x_j + \frac{d}{2}\right) / \left(z_j - \frac{h}{2}\right),$$

$$\theta_2 = \tan^{-1} \left(x_i - x_j + \frac{d}{2}\right) / \left(z_j - \frac{h}{2}\right),$$

$$\theta_3 = \tan^{-1} \left(x_i - x_j + \frac{d}{2}\right) / \left(z_j - \frac{h}{2}\right),$$

$$\theta_4 = \tan^{-1} \left(x_i - x_j + \frac{d}{2}\right) / \left(z_j - \frac{h}{2}\right),$$

Here G is the gravitational constant, d and h are the width and height of each block.

LINEAR INVERSION METHODOLOGY

In most of the inverse modeling cases, we deal with the underdetermined problems, i.e. the number of unknowns is much greater than the number of observed data. For a general underdetermined system of linear equations, i.e. $d=Pf$ where d is the column vector of the observed gravity field data, f is the column vector of the unknown, i.e. density, and P is the kernel rectangular matrix, the minimum norm solution is defined as the model that fits the data exactly which is given by (Menke, 1984):

$$f=P^T(PP^T)^{-1}d \tag{3}$$

we can solve the inversion problem using the standard damped least-squares method, as:

$$f=(P^TP+\gamma I)^{-1}P^Td \tag{4}$$

where γ is the damping parameter or regularization parameter, I is an identity matrix and the superscript T denotes the matrix transposition. The solution of equation (4) can be estimated by minimizing the following Tikhonov cost function:

$$S = \arg \min \{ \|d - Pf\|^2 + \gamma \|f\|^2 \}, \tag{5}$$

Analyzing this expression can be realized that the duty of the damping is minimizing the first term of equation (5) values to finding the model that gives the best fit to the data to Minimize the last

term values to obtain the model with the smallest norm. The choice of γ is usually determined by trial-and-error.

In order to stabilize the inversion, the singular value decomposition (SVD) technique is usually employed. The equation for singular value decomposition of matrix $P_{n \times m}$ is the following:

$$P = USV^T, \tag{6}$$

where S is an $n \times m$ left eigenvector matrix, U is an $n \times n$ diagonal matrix. The elements of $U_{n \times n}$ are only nonzero on the diagonal, and are called the singular values. V^T is also an $m \times m$ right eigenvector matrix and T stands for transpose. Note that $VV^T = V^T V = I_m$ and $UU^T = U^T U = I_n$. The singular values of matrix $P_{n \times m}$ are the positive entries of $U_{n \times n}$ which are distributed in decreasing order along its main diagonal and are equal to positive square roots of the eigenvalues (s_i) of the covariance matrices $P^T P$ & PP^T . P^{-1} and P^T are also, respectively:

$$P^{-1} = (USV^T)^{-1} = U^T S^{-1} V, \tag{7}$$

$$P^T = VSU^T, \tag{8}$$

Therefore, we can rewrite the equation 3 as:

$$(P^{-1}P)^{-1} P^T d = VS^{-2} V^T VSU^T d = VS^{-1} U^T d, \tag{9}$$

The singular value decomposition of matrix $P_{n \times m}$ can be also written as follows:

$$P = \sum_{i=1}^r u_i s_i v_i^T \tag{10}$$

where r is the rank of matrix $P_{n \times m}$, u_i is the i -th eigenvector of covariance matrix PP^T , v_i is the i -th eigenvector of covariance matrix $P^T P$, s_i is the i -th singular value of matrix $P_{n \times m}$ as $s_1 \geq s_2 \geq \dots \geq s_r > 0$, and is an $n \times m$ matrix of unitary rank called the i -th eigenimage of matrix $P_{n \times m}$.

On the basis of equation (10), the damped least-squares solution (equation 4) can be rewritten as the damped SVD, we will have:

$$f = \sum_{i=1}^r k_i \frac{u_i^T d}{s_i} v_i, \tag{11}$$

Here k_i is filter factor defined as

$$k_i = \frac{s_i}{(s_i + \gamma)}, \tag{12}$$

Usually, in the first iteration, the regularization parameter is considered to be a large positive value as at each iteration the damping factor is multiplied by a factor less than unity so that the least-

squares method reaches near a solution (Meju, 1994). According to Arnason and Hersir (1988) the damping factor is determined as follows:

$$\gamma = s_R \Delta d^{\frac{1}{R}}, \tag{13}$$

Where R is the iteration number for the damping factor at any iteration, s is the eigenvalue parameter and the term Δd is given by

$$\Delta d_r = \frac{(d_{r-1} - d_r)}{d_{r-1}}, \tag{14}$$

Where, d_{r-1} is the gravity misfit value obtained at previous iteration and d_r is the misfit computed at the current iteration. For $s_i \gg \gamma$, $k_i \approx 1$, thus it is clear that the components are little influenced by the damping factor and for $s_i \ll \gamma$, $k_i \approx 0$.

In inverting gravity data due to a causative mass, the evaluated density distribution related to a buried structure tend to concentrate near the surface. For nullifying the natural decay of the kernels and maximizing the depth resolution, a depth weighting function is included in the problem. Li and Oldenburg (1998) suggested to employ a depth weighting function such as:

$$w_z = \frac{1}{(z + z_0)} \tag{15}$$

where z is the depth of the layers and z_0 depends on the cell size of the model and the observation height of the gravity data.

In this paper, we employ the two-norm ($L2$ norm) as a criterion for stopping the iteration process in the inversion algorithms. The $L2$ norm has the form:

$$L2 \text{ norm: } \|e\|_2 = \left[\sum_k |e_k|^2 \right]^{1/2} \tag{16}$$

Where the e is the difference between the observed gravity data and inverted gravity data due to the evaluated model from the density distribution at each iteration. The best form of the under surface density distribution is obtained when the $L2$ norm in an iteration achieve the value less than the pre-defined value which in this case the iteration is terminated. Otherwise, the lowest amount estimated by the $L2$ norm during inversion process is considered as the best inverted under surface density distribution.

SYNTHETIC MODEL ANALYSIS WITH DAMPED SVD

Figure 2(a) shows the gravity response due to the assumed model shown in Figure 2(b) where the sub-surface ground has been partitioned into 15×10 prisms with the respective dimensions of $10 \text{ m} \times 5 \text{ m}$. As is shown in Figure 2(b), the 2D model include 6 prisms whose density contrast is 1000 kg/m^3 . The gravity effect corresponding to the resulting inverted causative body (Figure 2c), is displayed in Figure 2(a). This inverted model that is exactly similar to the original causative body, was obtained at 5th iteration, where the $L2$ norm as the stopping criterion attain the smallest amount.

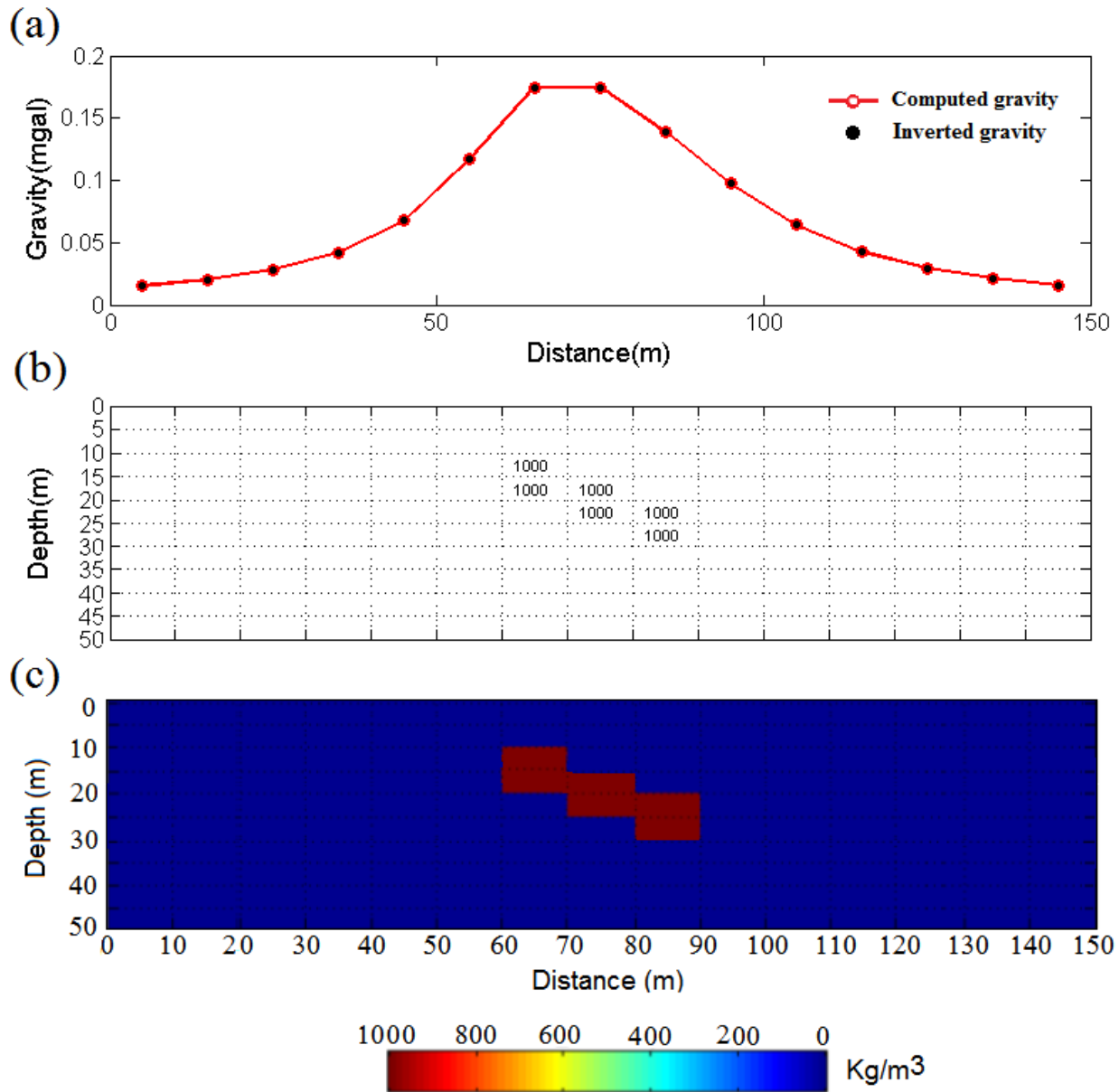


Figure 2. a) Computed and inverted gravity due to b) first assumed synthetic model and c) inverted model, respectively.

For testing the stability and sensitivity of the inversion method, we divided the subsurface inversion domain, Figure 2(b) into 75×25 blocks of dimension $2 \text{ m} \times 2 \text{ m}$ (Figure 3). Therefore, the whole domain is $150 \text{ m} \times 50 \text{ m}$ and the total number of blocks is $M=1875$.

Figure 4 shows the inferred density distribution from inverse modeling. The effect of error has been studied by adding 5% of random noise to the gravity response of the model shown in Figure 3. The inversion result is presented in Figure 5. These inverted models, i.e. figures 4 and 5, accrue at 7th and 10th iterations, respectively. Since, the inverted structures in both cases, with and without noise, are close to that of the assumed model, it can be concluded that the damped SVD inversion provides satisfactory results.

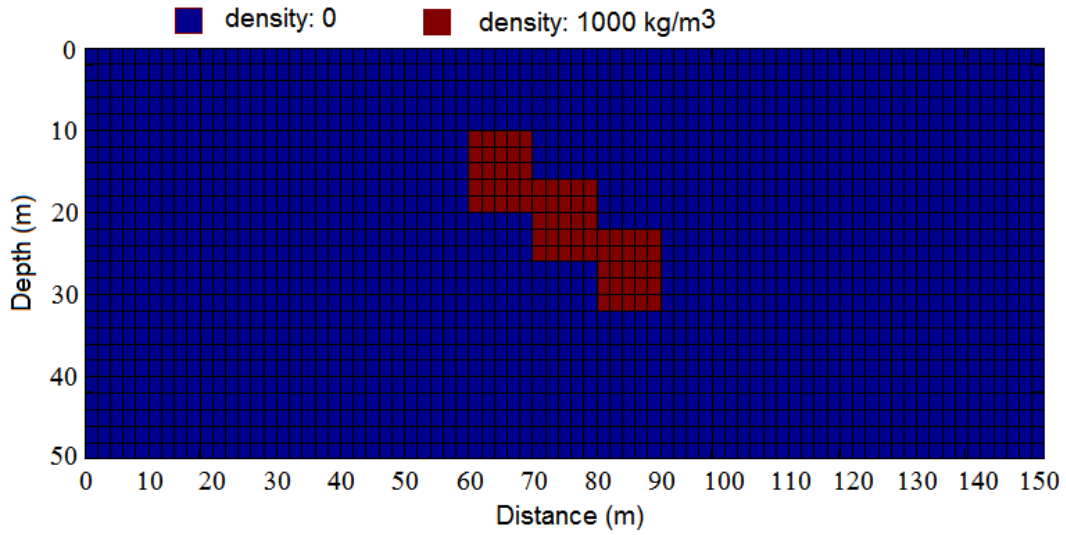


Figure 3. Second assumed density model in the inversion domain, which is constituted by 75×25 blocks with dimension 2 m × 2 m.

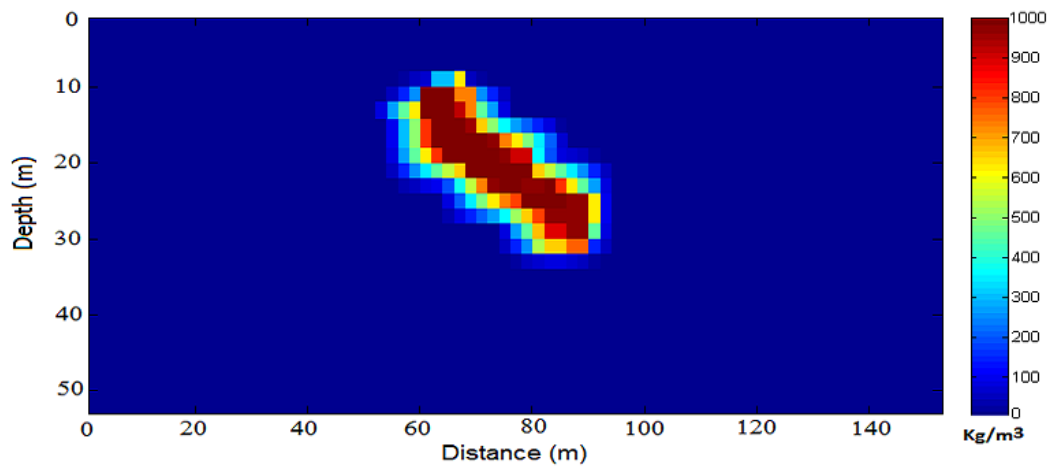


Figure 4. The obtained density distribution from inverting the gravity response of the second assumed model

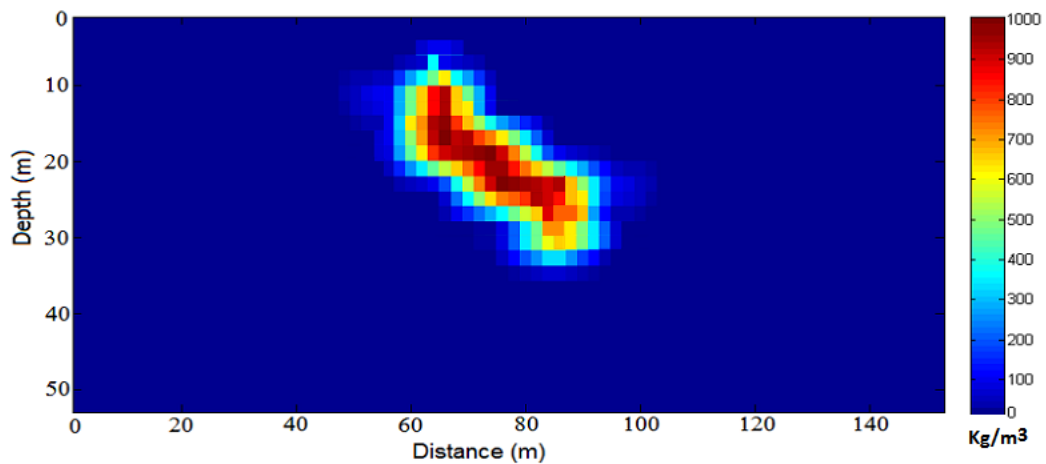


Figure 5. The obtained density distribution from inverting the gravity response of the second assumed model as corrupted with 5% random noise

GRAVITY OF DYKE MODEL

The gravity effects $g(i)$ of a finite dyke-like structure at a point $x(i)$ along a profile perpendicular to its strike direction which runs across the center of the target (Figure 6), is given in Telford and Geldart (1976) as

$$\begin{aligned}
 g(i) = 2G\rho w \frac{1}{2} \sin \theta \log & \frac{\left\{ (z + H \sin \theta)^2 + (x(i) + H \cos \theta)^2 + Y^2 \right\}^{\frac{1}{2}} - Y}{(z + H \sin \theta)^2 + (x(i) + H \cos \theta)^2 + Y^{\frac{1}{2}} + Y} \\
 & \times \frac{\left(x(i)^2 + z^2 + Y^2 \right)^{\frac{1}{2}} + Y}{\left(x(i)^2 + z^2 + Y^2 \right)^{\frac{1}{2}} - Y} \\
 - \cos \theta \tan^{-1} & \frac{Y(z \sin \theta + H + x(i) \cos \theta)}{\left\{ (z + H \sin \theta)^2 + (x(i) + H \cos \theta)^2 + Y^2 \right\}^{\frac{1}{2}} (x(i) \sin \theta - z \cos \theta)} \\
 + \cos \theta \tan^{-1} & \frac{Y(z \sin \theta + H + x(i) \cos \theta)}{\left\{ x(i)^2 + z^2 + Y^2 \right\}^{\frac{1}{2}} (x(i) \sin \theta - z \cos \theta)}
 \end{aligned} \tag{17}$$

Where the G is the gravitational constant, ρ is the density contrast, w is the thickness, θ is the dip angle of the dyke considered anticlockwise from horizontal, z is the depth to the top, $2Y$ is the strike length of the dyke and H is the dipping extent of the buried dyke.

NONLINEAR INVERSION METHODOLOGY

The inversion of gravity anomalies is implicitly a mathematical process, aimed at fitting the computed gravity anomalies to the observed ones in the least-squares approach and then estimating the four parameters namely the depth to top (z), width (thickness) (w), dip (slope) θ and dipping extent (height) (H). The process of the inversion begins by computing the theoretical gravity anomaly of the assumed simple geometry using equation (17). The difference between the observed gravity $g_{obs}(x_i)$, and calculated gravity anomaly of an initial assumed model $g_{cal}(x_i)$, can be estimated by a misfit function, J (Chakravarthi and Sundararajan, 2007), as

$$J = \sum_{i=1}^N \left[g_{obs}(x_i) - g_{cal}(x_i) \right]^2 \tag{18}$$

N is the number of observed gravity data. We have employed the Marquardt's algorithm (1963) given by Chakravarthi and Sundararajan (2006a) for minimizing the misfit function until the normal equations can be solved for overall modifications of the four unknown structural parameters, as

$$\sum_{i=1}^N \sum_{k=1}^4 \frac{\partial g(x_i)}{\partial a_j} \frac{\partial g(x_i)}{\partial a_k} (1 + \delta \lambda) da_k = \sum_{i=1}^N \left[g_{obs}(x_i) - g_{cal}(x_i) \right] \frac{\partial g(x_i)}{\partial a_j}, \text{ for } j = 1, \dots, 4 \tag{19}$$

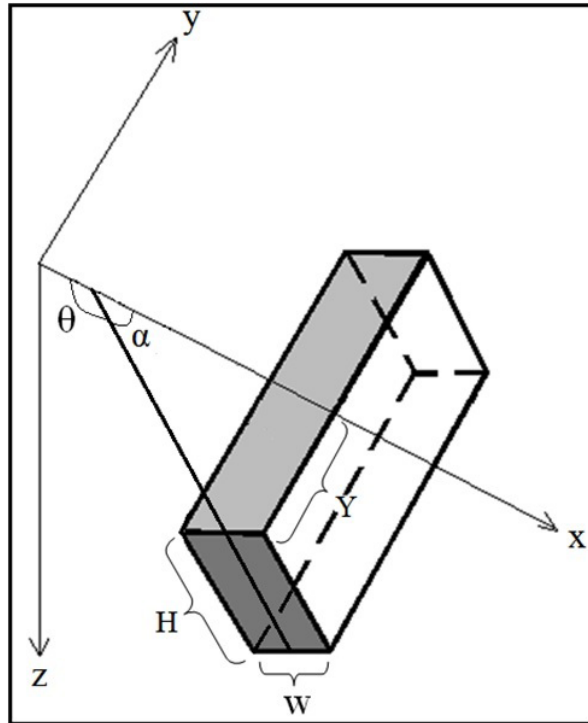


Figure 6. Geometry of a 3D dipping tabular target

where d_{a_k} , $k=1, 2, 3$ and 4 are applied to the four model parameters of the sheet-like geometry structure. Partial derivatives required in the above system of equation (19) are calculated by a numerical approach using Matlab. Also,

$$\delta = \begin{cases} 1 & \text{for } k = j, \\ 0 & \text{for } k \neq j, \end{cases}$$

and λ is the damping factor. The advancements, d_{a_k} , $k=1, 2, 3$ and 4 evaluated from equation (19) are then added to or subtracted from the available parameters estimated from last iteration and the process repeats until the misfit, J , in equation (18) descends below a predetermined allowable error or the damping factor obtains a large value which is greater than predefined amount or the repetition continues until the end of the considered number for iterations (Chakravarthi and Sundararajan, 2008).

SYNTHETIC MODEL ANALYSIS WITH MARQUARDT INVERSION

Figure 7(a) show the observed and calculated gravity anomalies due to the initial and assumed models which are shown in figure 7(b). The considered values for the density contrast is $\rho=1000 \text{ kg/m}^3$ and semi-length of the dyke strike is $Y=50 \text{ m}$, values that during inversion remain constant. The selected values for the parameters which improve during inversion, i.e. depth to top, width, dip and height for the initial model are 20 m , 15 m , 60° clockwise from the horizontal toward the right (i.e. α in Figure 1 or 120° anticlockwise from the horizontal (θ)) and 60 m , respectively and for the assumed model are 15 m , 12 m , 54° clockwise from the horizontal (i.e. α in Figure 6 or 36° from the vertical to the right) and 51 m , respectively.

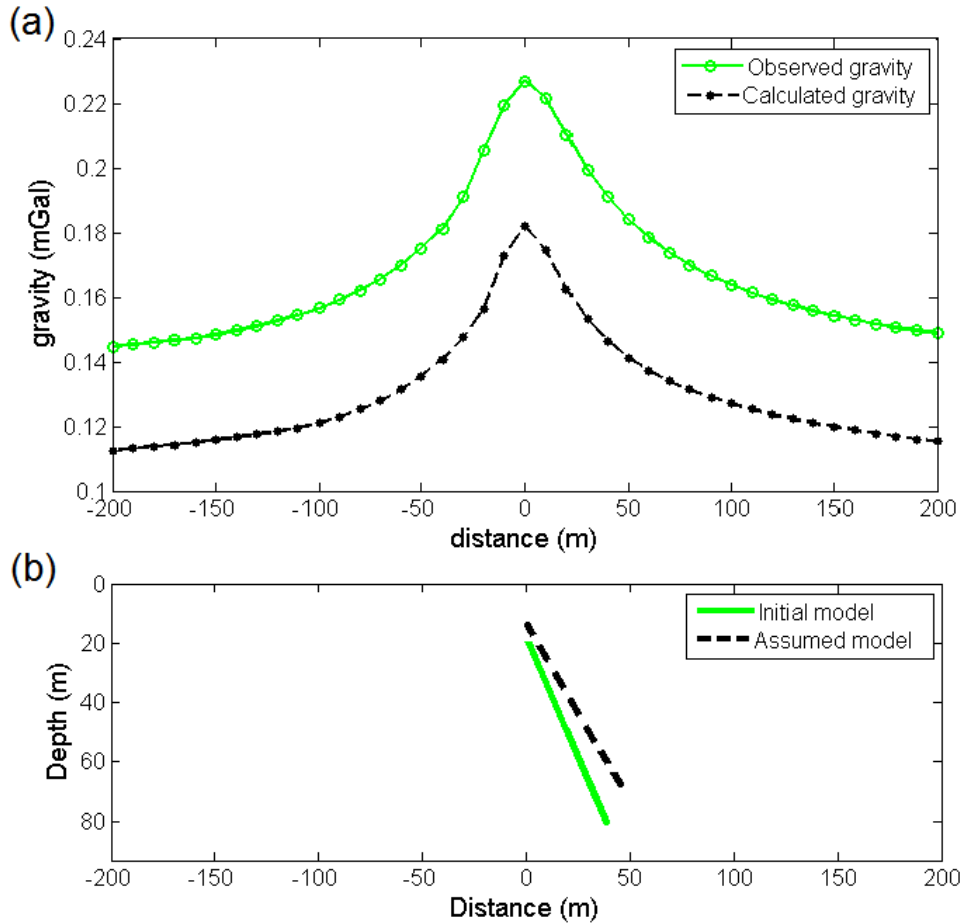


Figure 7. a) The observed and calculated gravity anomalies along a profile due to b) the initial ($z=20$ m, $w=15$ m, $\alpha=60$ degree and $H= 60$ m) and assumed ($z=15$ m, $w=12$ m, $\alpha=54$ degree and $H= 51$ m) models with a density contrast of 1000 kg/m^3

The predefined values for misfit function, J , iteration number and maximum damping factor (λ) are 10^{-4} mGal, 100 and 14, respectively. The initial damping factor is given as 0.5.

The misfit, J , reduces intensely from its initial value of 0.214 mGal at the first iteration to 0.000073 mGal at the end of the 6th iteration and then incrementally reaches 45×10^{-7} mGal at the 10th iteration (Figure 8e). Because the misfit, J , obtained at the 10th iteration was smaller than the allowable error value, the iteration process is ceases and therefore the optimum estimates for the depth, width, dip and height (dipping extend) are corresponding to the evaluated quantity at 9th iteration of the inverse modeling.

Figures 8(a), 8(b), 8(c) and 8(d) shows the variations of the model parameters, i.e. z , w , α and H versus the iteration number. The conclusive obtained parameters values are $z=19.98$ m, $w=15$ m, $\alpha=60.01$ degree and $H=59.97$ m.

Figure 9(a) exhibits the inverted gravity anomaly from the resulted model parameters which is shown in Figure 9(b). The percentage of error in the determination of the depth, width, dip and height parameters are 0.1, zero, about 0.017 m and 0.05, respectively. The considered parameters values and numerical results for the synthetic gravity data are tabulated in Tables 1.

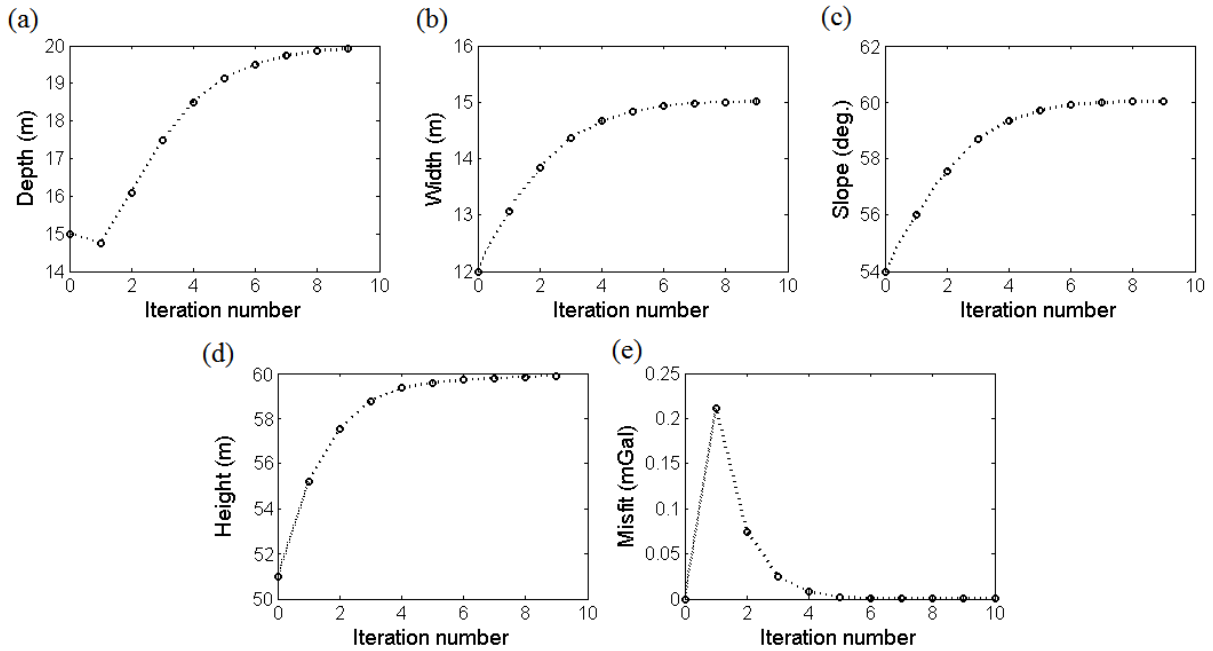


Figure 8. The variations of a) depth b) width c) dip d) height and e) misfit function versus iteration number for synthetic gravity data in figure 2.

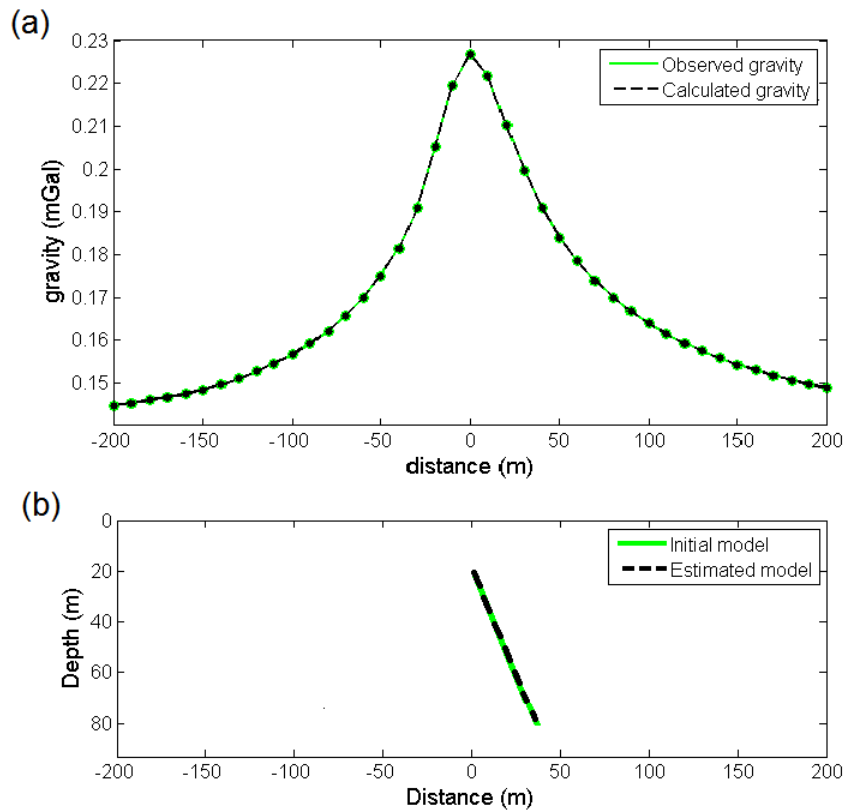


Figure 9. a) The observed and calculated gravity anomalies along a profile due to b) the initial ($z=20$ m, $w=15$ m, $\alpha=60$ degree and $H=60$ m) and estimated ($z=19.98$ m, $w=12$ m, $\alpha=60.01$ degree and $H= 59.97$ m) models with a density contrast of 1000 kg/m^3

Table 1. Numerical results obtained from the Marquardt inversion of the synthetic gravity data

Parameter	Depth (m)	Width (m)	Dip α (degree)	Height (m)
Initial	20	15	60	60
Assumed	15	12	54	51
Estimated	19.98	15	60.01	59.97
Error %	0.1	0	0.017	0.05
Iteration	9			
Misfit (mGal)	62×10^{-7}			

The effect of error has been evaluated by adding 10% random noise to the gravity response of the initial dyke model (Figure 7a) using the following expression:

$$g_{nois}(x_i) = g_{obs}(x_i) [1 + (RAN(i) - 0.5) \times 0.1] \tag{20}$$

where $g_{nois}(x_i)$ is the noise corrupted synthetic data at x_i , and RND (i) is a pseudorandom number whose range is between 0 to 1. The observed gravity data with added 10% random noise is shown in Figure 10(a). Furthermore, the initial and assumed models are shown in Figure 10(b). The considered values for the depth to top, width, dip and height parameters of the assumed model are given as 22 m, 13 m, 63° clockwise from the horizontal toward the right (i.e. $\alpha = 63^\circ$) and 63 m, respectively.

In noisy data case, the assigned values for misfit function, J , iteration and maximum damping factor (λ) are set as in the free-noise data case. The initial damping factor also is determined as 0.2.

The misfit, J , reduces quickly from its initial value of 0.0493 mGal at the first iteration to 0.0024 mGal at the end of the 5th iteration and then incrementally attains 0.0057 mGal after the 16th iteration (Figure 11e). The iteration finished at the 16th iteration where the damping factor value exceeded from the predefined value and reached a value of 24.62. The final values of the evaluated depth to top, width, dip and height at the 15th iteration are $z=19.9$ m, $w=14.7$ m, $\alpha=62.08$ degree and $H=61.5$ m, respectively (Figures 11a to 11d). The percentage of error in the estimation of the depth to top, width, dip and height are 0.1, 2, about 3.67 and 2.5, respectively.

Figure 12(a) shows the inverted gravity anomaly calculated from the inverted model parameters which is shown in Figure 12(b). The theoretical parameters and inferred values for the noise corrupted synthetic gravity data have been summarized in Table 2.

To investigate the solutions constancy and performance of the Marquardt inversion, two different initial and assumed dyke models were assumed to analyze the gravity anomalies related to them with and without a random noise of 10% (Table 3 and 4). The estimated structural parameters are almost correspond to the initial ones.

REAL GRAVITY ANALYSIS

Real gravity data are from the Zereshlu Mining Camp, situated in the west of Mianeh, East Azerbaijan Province, Iran. The main mineral in this area is Manganese which exists mostly in the form of vein deposit or sheet-like structure with the origin of the hydrothermal.

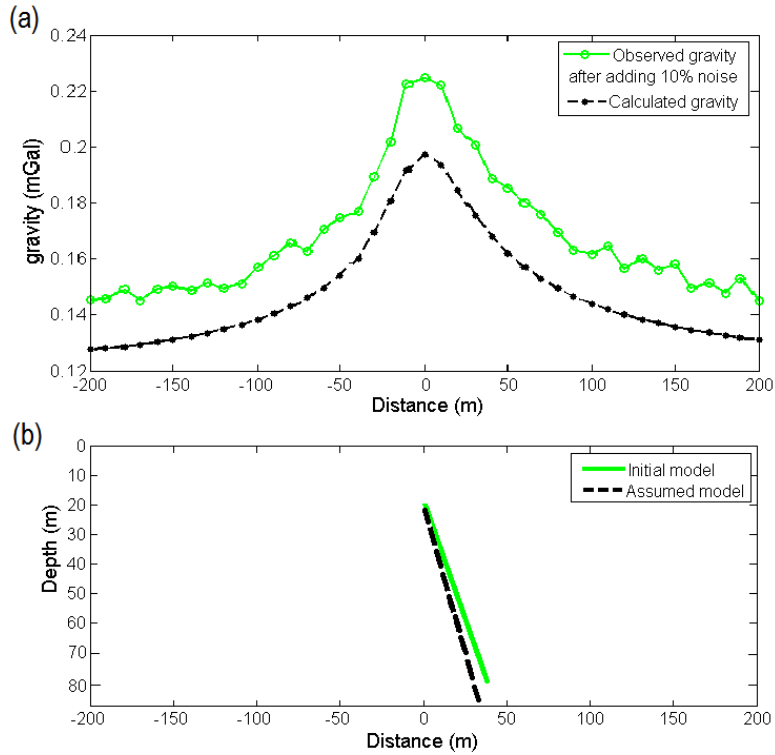


Figure 10. a) The observed gravity anomaly with a added random noise of 10% and calculated gravity anomaly along a profile due to b) the initial ($z=20$ m, $w=15$ m, $\alpha=60$ degree and $H= 60$ m) and assumed ($z=22$ m, $w=13$ m, $\alpha=63$ degree and $H= 63$ m) models with a density contrast of 1000 kg/m^3

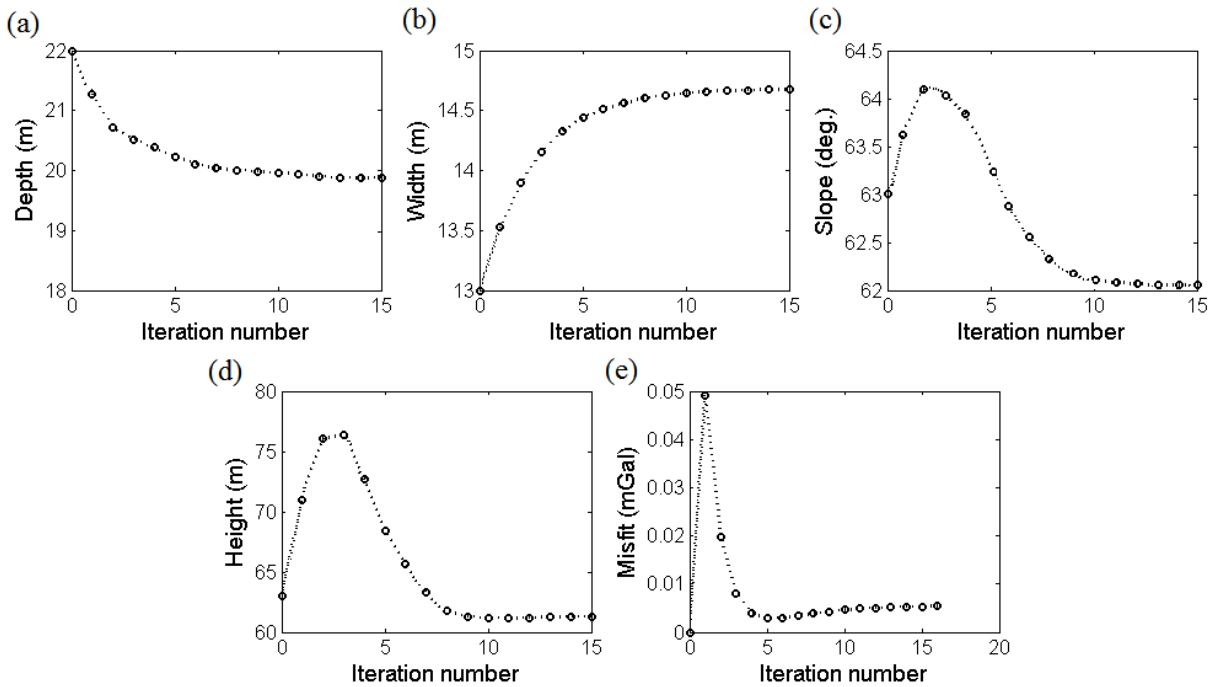


Figure 11. Variations of a) depth b) width c) dip d) height and e) misfit function versus iteration number for 10% noise corrupted synthetic gravity data shown in figure 5.

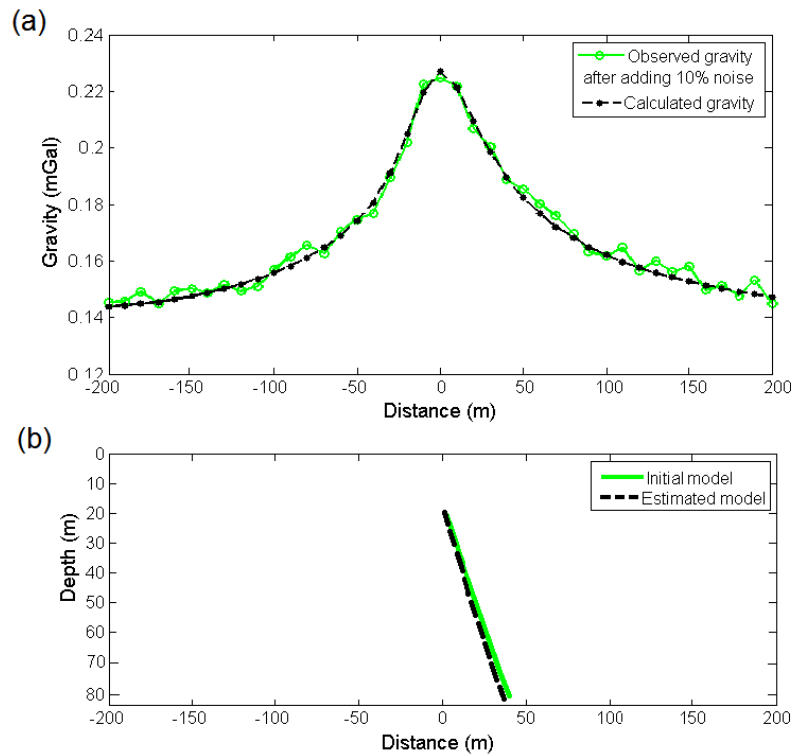


Figure 12. a) The observed gravity anomaly with a added random noise of 10% and calculated gravity anomaly along a profile due to b) the initial ($z=20$ m, $w=15$ m, $\alpha=60$ degree and $H= 60$ m) and estimated ($z=19.9$ m, $w=14.7$ m, $\alpha=62.08$ degree and $H= 61.5$ m) models with a density contrast of 1000 kg/m^3

Table 2. Numerical results obtained from the Marquardt inversion of the noise corrupted synthetic gravity data

Parameter	Depth (m)	Width (m)	Dip α (degree)	Height (m)
Initial	20	15	60	60
Assumed	22	13	63	63
Estimated	19.9	14.7	62.08	61.5
Error %	0.1	2	3.67	2.5
Iteration	15			
Misfit (mGal)	0.0053			

Table 3. Inverted parameters from analysis of free-noise gravity anomalies for different models

Parameter	With 10% random noise							
	Model 1				Model 2			
	Depth (m)	Dip (deg)	Width (m)	Height (m)	Depth (m)	Dip (deg)	Width (m)	Height (m)
Initial	25	50	12	45	40	110	20	65
Assumed	30	60	16	40	32	100	14	58
Estimated	25.01	49.97	11.99	45.02	39.97	110.1	20.02	65.03
Error %	0.04	0.06	0.083	0.044	0.075	0.091	0.1	0.046
Misfit (nT)	0.00000072				0.00000094			
Lambda λ	2.4×10^{-12}				5.7×10^{-23}			
Iteration	12				18			

Table 4. Inverted parameters from analysis of 10% noise-corrupted gravity anomalies for different models

Parameter	With 10% random noise							
	Model 1				Model 2			
	Depth (m)	Dip (deg)	Width (m)	Height (m)	Depth (m)	Dip (deg)	Width (m)	Height (m)
Initial	25	50	12	45	40	110	20	65
Assumed	30	60	16	40	32	100	14	58
Estimated	25.2	50.3	11.85	45.13	38.84	112.6	19.6	66.8
Error %	0.04	0.06	0.083	0.044	2.9	2.36	2	2.77
Misfit (nT)	0.000086				0.078			
Lambda λ	7.1×10^{-18}				32.8			
Iteration	19				23			

Figure 13 exhibits the geological map of the region around the Zereshlu mine. The gravity measurement region is indicated by a black circle. The predominant rocks in the region under investigation are the conglomerate, sandstone and silt. As well as, in this region there are the layers of the basalt, andesite and altered andesite with ferrous oxide. These rocks are considered as the host rocks of the manganese dioxide mineral which is thought to have filled the major faults and fractures. The net density of manganese dioxide is 4.75 gr/cm^3 and the average density of the basalt and andesite are about 2.9 gr/cm^3 and 2.6 gr/cm^3 , respectively. When the ferrous oxide and manganese dioxide are dispersed in the basalt and andesite, therefore, the density of the host rock and that of the target, can consider between 3.2 gr/cm^3 to 3.5 gr/cm^3 . The background density of the study area is about 2.6 gr/cm^3 , thus the density contrast between the body causative of gravity anomalies, i.e. the host rocks, and background domain range between 0.6 gr/cm^3 to 0.9 gr/cm^3 (on average 0.75 gr/cm^3).

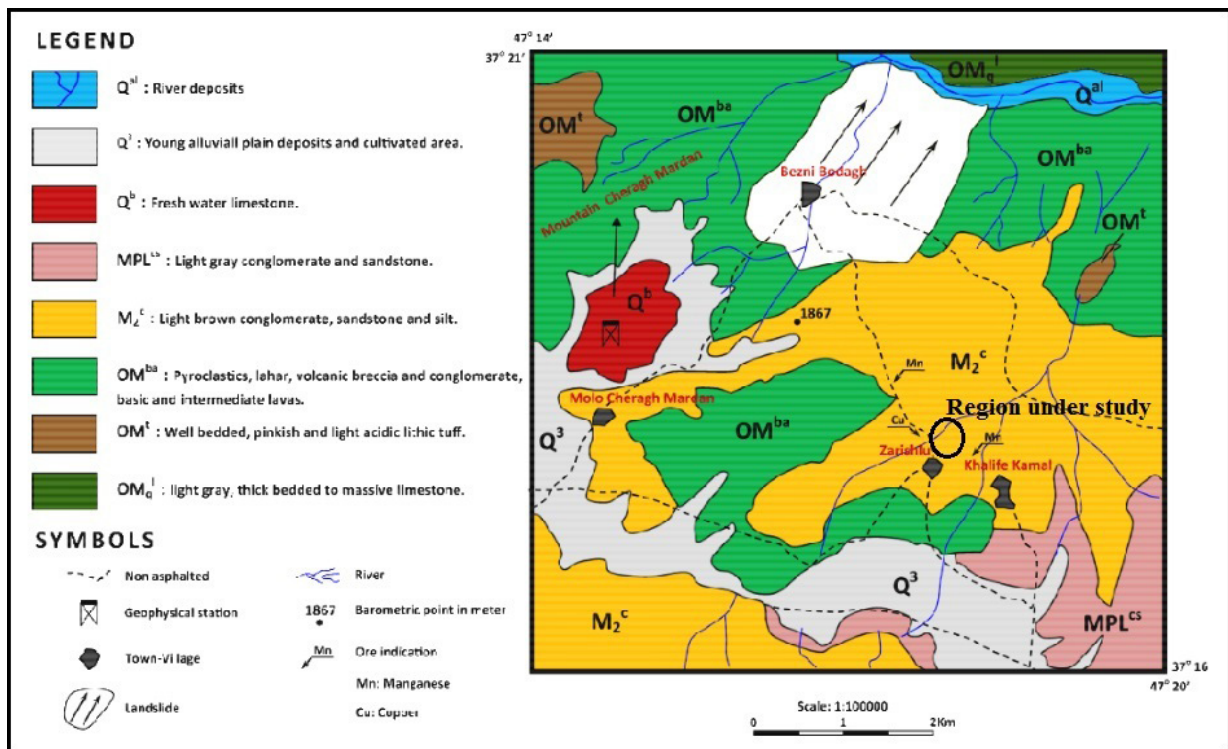


Figure 13. The geological map of the region under investigation

The gravity survey district in zone 38, stretches the UTM coordinate from 704410 m to 704555 m East and from 4130820 m to 4131000 m North. The Bouguer gravity anomaly map of the study area is shown in Figure 14. After removing the effect of regional gravity field from the Bouguer gravity anomaly, the residual gravity anomalies map is achieved (Figure 15). The linear gravity anomalies whose values are positive indicate the sources that are rich in the Manganese. The gravity sampling was performed at 33 points with an interval of 1.03 m along the 34 m profile AA', which runs across the dyke-like structure in the W-E direction (Figure 15). We apply the variations of the residual gravity field at the observed points over the profile AA' for reconstructing the buried structure.

For inverting the real gravity data (Figure 17a) using the damped SVD technique, the underground study domain was divided into $33 \times 17 = 561$ rectangular prisms with respective dimensions of 1.5×2.5 m. Figure 16 shows the density distribution that resulted from the linear inversion. The blocks whose densities are between 3.2 gr.cm^3 to 3.5 gr/cm^3 foreshow the manganese deposit body.

Inversion of the observed gravity data (Figure 17a) using the Marquardt inversion technique, we assume an initial model whose parameters values are given as $z=8$ m, $w=17$ m, $\alpha=38$ degree and $H=19$ m (Figure 17c). The calculated gravity due to the assumed model is shown in Figure 17(a). Moreover, the assigned values for misfit (J), iteration and damping factor (λ) are 0.0005 nmGal, 50 and 15, respectively.

The changes of each parameter and misfit against the iteration number during the inversion process are shown in Figures 18(a) to 18(d). The algorithm performed 10 iterations, before it ceased, since

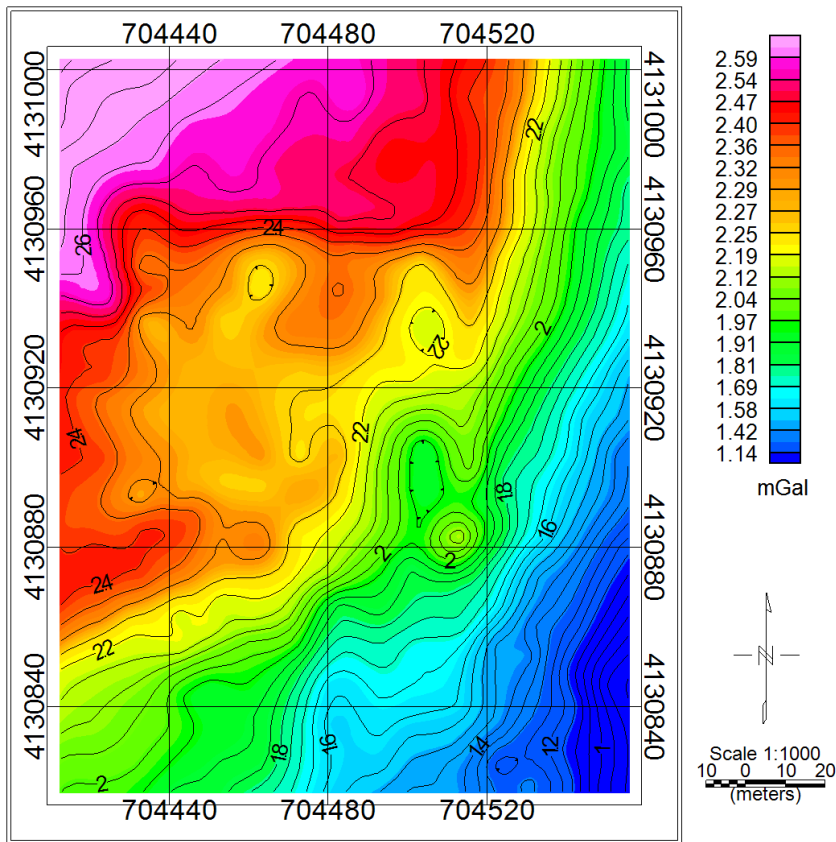


Figure 14. The Bouguer gravity anomaly map of the study district

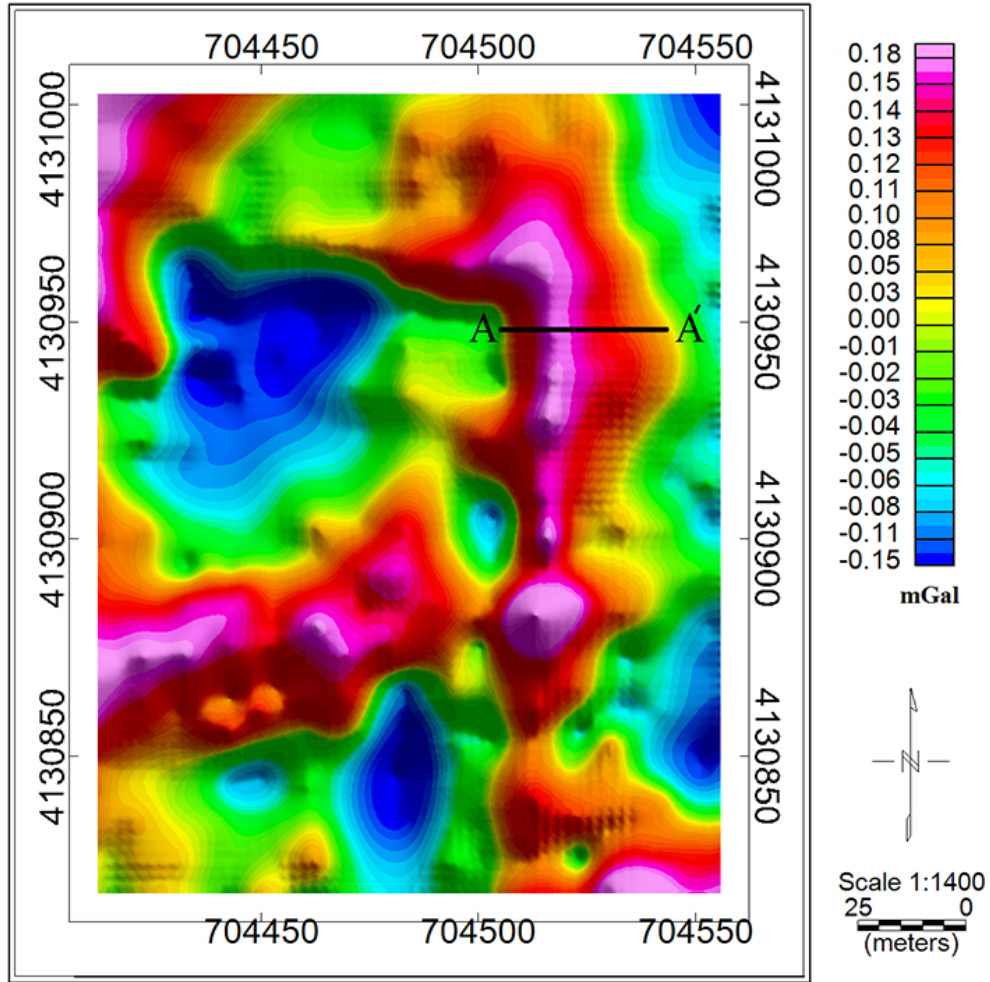


Figure 15. The residual gravity anomalies map of the study district. The profile AA' is specified in W-E direction.

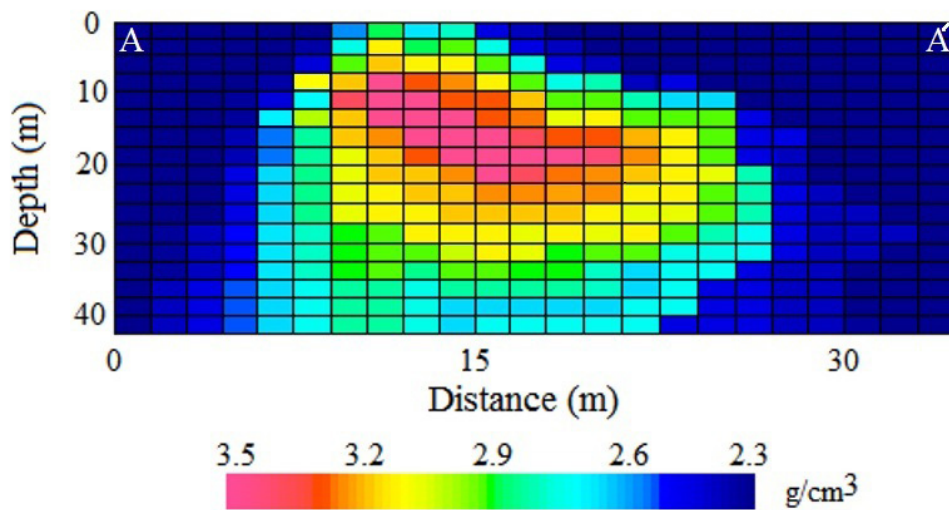


Figure 16. The inverted density distribution by inverting the real gravity data using damped SVD.

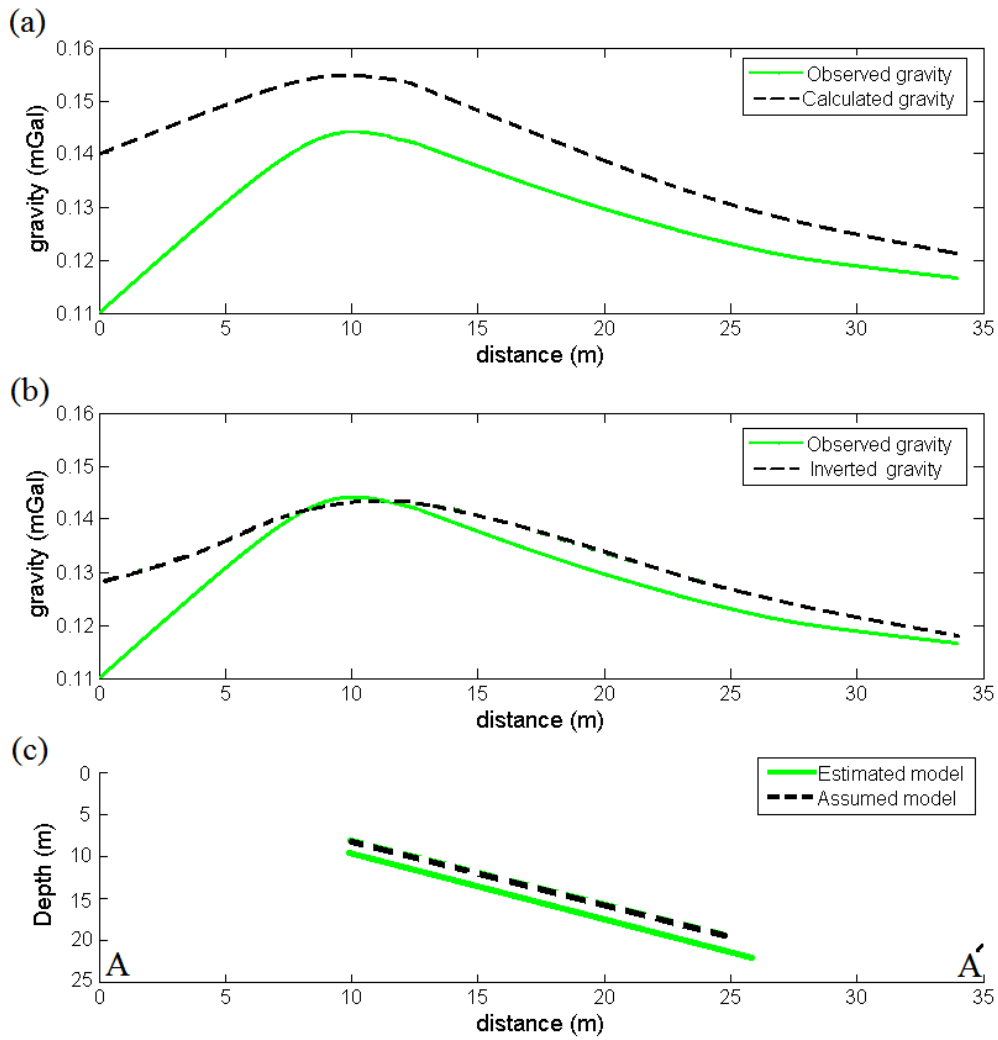


Figure 17. A) The observed gravity along the profile AA' and calculated gravity due to the assumed model, b) Inferred gravity from estimated structure, c) The assumed model and estimated model obtained by the Marquardt inversion.

Table 5. The initial parameters values and final parameters values from interpretation of the real gravity data

Parameter	Depth (m)	Width (m)	Dip α (deg)	Height (m)
Assumed	8	17	38	19
Estimated	9.4	15.8	38.04	20.3
Final Misfit (mGal)		0.00122		
Final Lambda λ		24.68		
Iteration		10		

at the end of this iteration number, the damping factor reached a value greater than the predefined value (see Table 5).

The misfit function variations versus the iteration number (Figure 18e) show a fast decrease from its first value of 0.00015 mGal to its value at the 3th iteration and then increase continually until 10th iteration whose value is 0.000127 mGal. The depth and height parameters increase steadily from its initial value to their final values at the 10th iteration whose values are 9.4 m and 20.3 m, respectively (Figures 18a and 18d). The width parameter decreases significantly until 6th iteration and then gradually achieved 15.8 m at the 10th iteration (Figure 18b). The dip parameter reduces from its initial value to its value at the 3th iteration and then increased rapidly until 10th iteration where it was obtained a value of 38.04 degree towards the east (Figure 18c). The resulted tabular model is delineated in Figure 17 (c). The gravity response estimated from the inferred parameters for the dyke-like structure (Figure 17c) is shown in Figure 17(b). The inverted structural parameters are given in Table 5.

DISCUSSION AND CONCLUSIONS

In this paper, we have introduced two inverse modeling methods, based on the damped singular value decomposition (DSVD) as a linear inversion and the Marquardt optimization algorithm as a nonlinear inversion. The Marquardt optimization algorithm has been developed for interpreting the gravity data due to a dyke-like structure. The validation and performance of the both approaches

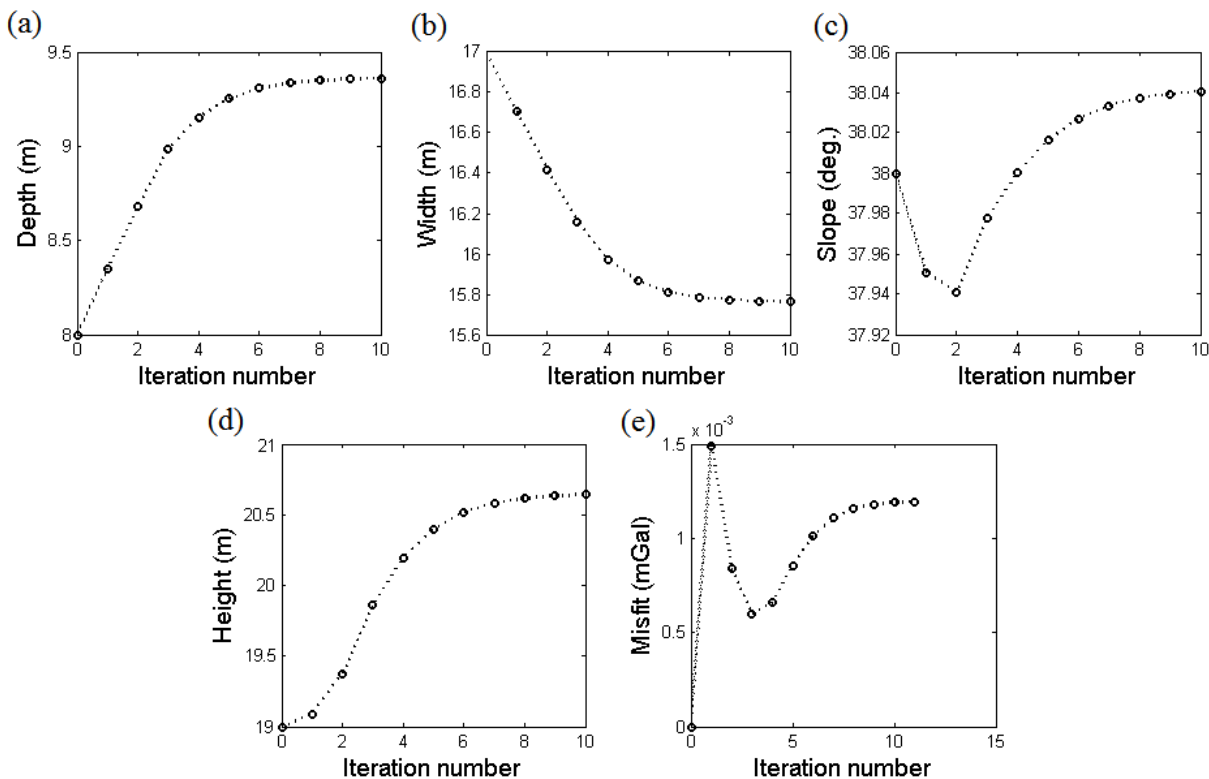


Figure 18. The variations of a) depth b) width c) dip d) height and e) misfit function versus iteration number for the real gravity data.

were evaluated using the theoretical gravity data, with and without random noise. The inverted models obtained from the analysis of the synthetic gravity data via the both methods are exactly similar to the initial ones. The Marquardt inversion shows an acceptable convergence for the various assumed parameters. We employed the both methods for inverting the real gravity data due to a near surface sheet-like structure from Iran. In the resulted density distribution by the damped SVD inversion, the adjacent blocks with a density bigger than 3.2 gr/cm^3 , demonstrate the geometry of the Manganese ore deposit. Considering to inverted density distribution, the depth to the top and bottom of the simulated structure with a direction of NW-SE, are about 7.5 m and 25 m, respectively. Moreover, the average amount of width and extension of the interpreted structure are given about 15 m and 22 m, respectively. As the distribution density resulted from the damped SVD inversion demonstrate a subsurface dyke-like structure, therefore, we can apply the Marquardt optimization algorithm for analyzing the gravity data. The inferred parameters using the Marquardt inversion of the real gravity data demonstrate a dyke-like structure with a width of 15.8 m, a dip of 38.04 degree and a height (extension) of 20.3 m where the depth to the top and bottom are 9.4 m and 21.9 m, respectively.

The comparison of the parameters values of the inverted structures from the damped SVD inversion and the Marquardt optimization method shows a close affinity between them. Therefore, using from the both inversion methods can be a helpful and advantageous strategy in the accurate interpretation of the gravity data.

REFERENCES

- Abdelfattah A.K., Jallouli C., Fnais M., Qaysi S., Alzahrani H., Mogren S., 2021, The key role of conjugate fault system in importing earthquakes into the eastern flank of the Red Sea. *Earth, Planets and Space*, 73, 178.
- Abdelrahman E.M., 1990, Discussion on "A least-squares approach to depth determination from gravity data" by O. P. Gupta. *Geophysics*, 55, 376-378.
- Abdelrahman E.M., Abo-Ezz E.R., Essa K.S., El-Araby T.M., Soliman K.S., 2007, A new least-squares minimization approach to depth and shape determination from magnetic data. *Geophysical Prospecting*, 55, 433-446.
- Abdelrahman E.M., Bayoumi A.I., Abdelhady Y.E., Gobashy M.M., El-Araby H.M., 1989, Gravity interpretation using correlation factors between successive least-squares residual anomalies. *Geophysics*, 54, 1614-1621.
- Abdelrahman E.M., Bayoumi A.I., El-Araby H.M., 1991, A least-squares minimization approach to invert gravity data. *Geophysics*, 56, 115-118.
- Abdelrahman E.M., El-Araby H.M., 1993, Shape and depth solutions from gravity using correlation factors between successive least-squares residuals. *Geophysics*, 59, 1785-1791.
- Abdelrahman E.M., El-Araby H.M., El-Araby T.M., Abo-Ezz E.R., 2001a, Three least squares minimization approaches to depth, shape, and amplitude coefficient determination from gravity data. *Geophysics*, 66, 1105-9.
- Abdelrahman E.M., El-Araby T.M., 1993, A least-squares minimization approach to depth determination from moving average residual gravity anomalies. *Geophysics*, 58, 1779-1784.

- Abdelrahman E.M., El-Araby T.M., El-Araby H.M., Abo-Ezz E.R., 2001b, A new method for shape and depth determinations from gravity data. *Geophysics*, 66, 1774–1778.
- Abdelrahman E.M., El-Araby T.M., Essa K.S., 2003, Shape and depth solutions from third moving average residual gravity anomalies using window curves method. *Kuwait J. Sci. Eng.*, 30, 95–108.
- Abdelrahman E.M., Essa K.S., 2005, Magnetic interpretation using a least-squares curves method. *Geophysics*, 70, L23–L30.
- Abdelrahman E.M., Essa K.S., 2015, A new method for depth and shape determinations from magnetic data. *Pure and Applied Geophysics*, 172, 439–460.
- Abdelrahman E.M., Essa K.S., El-Araby T.M., Abo-Ezz E.R., 2015, Depth and shape solutions from second moving average residual magnetic anomalies. *Exploration Geophysics*, 47(1) 58–66.
- Abdelrahman E.M., Sharafeldin S.M., 1996, An iterative least-squares approach to depth determination from residual magnetic anomalies due to thin dikes. *Journal of Applied Geophysics*, 34, 213–220.
- Al-Garni M.A., 2013, Inversion of residual gravity anomalies using neural network. *Arab. J. Geosci.*, 6, 1509–1516.
- Arnason K., Hersir G.P., 1988, One dimensional inversion of Schlumberger resistivity soundings. Computer Program, Description and User's Guide: The United Nations University, Geothermal Training, Report 8, 59 pp.
- Asfahani J., and Tlas M., 2008, An automatic method of direct interpretation of residual gravity anomaly profiles due to spheres and cylinders. *Pure and Applied Geophysics*, 165(5), 981–994.
- Asfahani J., Tlas M., 2007, A robust nonlinear inversion for the interpretation of magnetic anomalies caused by faults, thin dikes and sphere like structure using stochastic algorithms. *Pure and Applied Geophysics*, 164, 2023–2042.
- Ateya I.L., Takemoto, S., 2002, Gravity inversion modeling across a 2-D dike-like structure-A Case Study. *Earth Planets Space*, 54, 791–796.
- Bastani M., Pedersen L.B., 2001, Automatic interpretation of magnetic dike parameters using the analytical signal technique. *Geophysics*, 66, 551–561.
- Biswas A., 2016. Interpretation of gravity and magnetic anomaly over thin sheet-type structure using very fast simulated annealing global optimization technique. *Modeling Earth Systems and Environment*, 2(1), 30.
- Biswas A., Parija M.P., Kumar S., 2017, Global nonlinear optimization for the interpretation of source parameters from total gradient of gravity and magnetic anomalies caused by thin dyke. *Annals of Geophysics*, 60, 2, G0218.
- Bosch M., McGaughey J., 2001, Joint inversion of gravity and magnetic data under lithological constraints. *The Leading Edge*, 20, 877–881.
- Bosch M., Meza R., Jiménez R., Hönig A., 2006, Joint gravity and magnetic inversion in 3D using Monte Carlo methods. *Geophysics*, 71(4), G153–G156.
- Chakravarthi V., Sundararajan N., 2004, Ridge regression algorithm for gravity inversion of fault structures with variable density. *Geophysics*, 69, 1394–1404.

- Chakravarthi V., Sundararajan N., 2006a, Gravity anomalies of multiple prismatic structures with depth-dependent density – A Marquardt inversion. *Pure and Applied Geophysics*, 163, 229–242.
- Chakravarthi V., Sundararajan N., 2007, Marquardt optimization of gravity anomalies of anticlinal and synclinal structures with prescribed depth-dependent density. *Geophysical Prospecting*, 55, 571–587.
- Chakravarthi V., Sundararajan N., 2008, TODGINV—A code for optimization of gravity anomalies due to anticlinal and synclinal structures with parabolic density contrast. *Computers & Geosciences*, 34, 955–966.
- Cooper G.R.J., 2012, The semi-automatic interpretation of magnetic dyke anomalies. *Computers & Geosciences*, 44, 95–99.
- Cooper G.R.J., 2014, The automatic determination of the location and depth of contacts and dykes from aeromagnetic data. *Pure and Applied Geophysics*, 171, 2417–2423.
- Cooper G.R.J., 2015, Using the analytic signal amplitude to determine the location and depth of thin dikes from magnetic data. *Geophysics*, 80, J1–J6.
- Eshaghzadeh A., 2017, Depth Estimation Using the Tilt Angle of Gravity Field due to the Semi-Infinite Vertical Cylindrical Source. *Journal of Geological Research*, Article ID 3513272, 7 pages.
- Eshaghzadeh A., Hajian A., 2018, 2-D inverse modeling of residual gravity anomalies from Simple geometric shapes using Modular Feed-forward Neural Network. *Annals of Geophysics*, 61,1, SE115.
- Eshaghzadeh A., Kalantary R.A., 2015, Anticlinal Structure Modeling with Feed Forward Neural Networks for Residual Gravity Anomaly Profile. 8th congress of the Balkan Geophysical Society, doi: 10.3997/2214-4609.201414210.
- Eslam E., Salem A., Ushijima K., 2001, Detection of cavities and tunnels from gravity data using a neural network. *Explor. Geophys.*, 32, 204–208.
- Essa K.S., 2007, A simple formula for shape and depth determination from residual gravity anomalies. *Acta Geophysica*, 55(2), 182–190.
- Essa K.S., 2012, A fast interpretation method for inverse modelling of residual gravity anomalies caused by simple geometry. *Journal of Geological Research*, Article ID 327037.
- Essa K.S., 2013, New fast least-squares algorithm for estimating the best-fitting parameters due to simple geometric-structures from gravity anomalies. *Journal of Advanced Research*. <http://dx.doi.org/10.1016/j.jare.2012.11.006>.
- Farquharson C.G., Ash M.R., Miller H.G., 2008, Geologically constrained gravity inversion for the Voisey's Bay ovoid deposit. *The Leading Edge*, 27, 64–69.
- Gallardo L.A., Meju M., 2003, Characterization of heterogeneous near-surface materials by joint 2D inversion of DC and seismic data. *Geophysical Research Letters*, 30, L1658.
- Gupta O.P., 1983, A least-squares approach to depth determination from gravity data. *Geophysics*, 48, 357–360.
- Hammer S., 1977, Graticule spacing versus depth discrimination in gravity interpretation. *Geophysics*, 42, 60–65.

Heincke B., Jegen M., Moorkamp M., Chen J., Hobbs, R.W., 2010, Adaptive coupling strategy for simultaneous joint inversions that use petrophysical information as constraints, 80th Annual International Meeting. SEG, Expanded Abstracts, 29, 2805–2809.

Ialongo S., Fedi M., Florio G., 2014, Invariant models in the inversion of gravity and magnetic fields and their derivatives. *Journal of Applied Geophysics*, 110, 51-62.

Kamm J., Lundin I.A., Bastani M., Sadeghi M., Pedersen L.B., 2015, Joint inversion of gravity, magnetic, and petrophysical data—A case study from a gabbro intrusion in Boden, Sweden. *Geophysics*, 80(5), B131–B152.

Last B.J., Kubik K., 1983, Compact gravity inversion. *Geophysics*, 48, 713-721.

Lelièvre P.G., Farquharson C.G., Hurich C.A., 2012, Joint inversion of seismic travel times and gravity data on unstructured grids with application to mineral exploration. *Geophysics*, 77, K1–K15.

Lines L.R., Treitel S., 1984, A review of least-squares inversion and its application to geophysical problems. *Geophys. Prosp.*, 32, 159-186.

Li Y., Oldenburg D.W., 1998, 3-D inversion of gravity data. *Geophysics*, 63, 109-119.

Marquardt D.W., 1963, An algorithm for least-squares estimation of nonlinear parameters. *Journal of the Society of Indian Applied Mathematics*, 11, 431–441.

Meju M.A., 1994, Geophysical data analysis: Understanding Inverse Problem Theory and Practice, Society of Exploration Geophysics Course Notes Series, 1st edn., No. 6, SEG publishers, Tulsa, Oklahoma, 296 pp.

Menke W., 1984, Geophysical data Analysis: Discrete Inverse Theory, Academic Press, Inc., New York.

Mohan N.L., Anandababu L., Rao, S., 1986, Gravity interpretation using the Melin transform. *Geophysics*, 51, 114-122.

Odegard M.E., Berg, J.W., 1965, Gravity interpretation using the Fourier integral. *Geophysics*, 30, 424-438.

Oldenburg D.W., 1974, The inversion and interpretation of gravity anomalies. *Geophysics*, 39(4), 526-536.

Osman O., Muhittin A.A., Ucan, O.N., 2007, Forward modeling with Forced Neural Networks for gravity anomaly profile. *Math. Geol.*, 39, 593-605.

Osman O., Muhittin A.A., Ucan O.N., 2006, A new approach for residual gravity anomaly profile interpretations: Forced Neural Network (FNN). *Annals of Geophysics*, 49, 6.

Parker R.L., 1972, The Rapid Calculation of Potential Anomalies. *Geophysical Journal of the Royal Astronomical Society*, 31, 447-455.

Peace A.L., Welford J.K., Geng M., Sandeman H., Gaetz B.D., Ryan S.S., 2018, Structural geology data and 3-D subsurface models of the Budgell Harbour Stock and associated dykes, Newfoundland, Canada. *Data in Brief*, 21, 1690-1696.

Peace A.L., Welford J.K., Geng M., Sandeman H., Gaetz B.D., Ryan S.S., 2018, Structural geology data and 3-D subsurface models of the Budgell Harbour Stock and associated dykes, Newfoundland, Canada. *Data in Brief*, 21, 1690-1696.

- Pilkington M., 2006, Joint inversion of gravity and magnetic data for two layer models. *Geophysics*, 71(3), L35–L42.
- Shamsipour P., Chouteau M., Marcotte D., 2011, 3D stochastic inversion of magnetic data. *Journal of Applied Geophysics*, 73, 336–347.
- Shamsipour P., Marcotte D., Chouteau M., 2012, 3D stochastic joint inversion of gravity and magnetic data. *Journal of Applied Geophysics*, 79, 27–37.
- Shamsipour P., Marcotte D., Chouteau M., Keating P., 2010, 3D stochastic inversion of gravity data using cokriging and cosimulation. *Geophysics*, 75, I1–I10.
- Sharma B., Geldart L.P., 1968, Analysis of gravity anomalies of two-dimensional faults using Fourier transforms. *Geophys. Prosp.*, 77-93.
- Shaw R.K., Agarwal N.P., 1990, The application of Walsh transforms to interpret gravity anomalies due to some simple geometrically shaped causative sources: A feasibility study. *Geophysics*, 55, 843-850.
- Skeels D.C., 1947, Ambiguity in gravity interpretation. *Geophysics*, 12, 43-56.
- Telford W.M., Geldart L.P., 1976, *Applied Geophysics*. Cambridge University Press, Cambridge.
- Tlas M., Asfahani J., 2011a, Fair function minimization for interpretation of magnetic anomalies due to thin dikes, spheres and faults. *Journal Applied Geophysics*, 75, 237–243.
- Tlas M., Asfahani J., 2011b, A new best-estimate methodology for determining magnetic parameters related to field anomalies produced by buried thin dikes and horizontal cylinder-like structures. *Pure and Applied Geophysics*, 168, 861–870.
- Tschirhart V., Jefferson C.W., Morris W.A., 2017, Basement geology beneath the northeast Thelon Basin, Nunavut: insights from integrating new gravity, magnetic and geological data. *Geophysical Prospecting*, 65, 617-636.
- Tschirhart V., Morris W.A., Jefferson C.W., Keating P., White J.C., Calhoun, L., 2013, 3D geophysical inversions of the north-east Amer Belt and their relationship to the geologic structure. *Geophysical Prospecting*, 61, 547–560.
- Tsuboi C., 1983, *Gravity*, 1st edn. George Allen & Unwin Ltd, London, 254 pp.
- Williams N.C., 2008, Geologically-constrained UBC-GIF gravity and magnetic inversions with examples from the Agnew-Wiluna Greenstone Belt, Western Australia. Ph.D. thesis, University of British Columbia.
- Zeyen H., Pous H., 1993, 3-D joint inversion of magnetic and gravimetric data with a priori information. *Geophysical Journal International*, 112, 244–256.